Commun Nonlinear Sci Numer Simulat 156 (2026) 109645

Contents lists available at ScienceDirect

Communications in Nonlinear Science and Numerical Simulation

journal homepage: www.elsevier.com/locate/cnsns

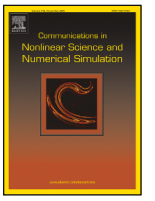

Research paper

On a negative chemotaxis system with lethal interaction

Federico Herrero-Hervás [a,b,*], Mihaela Negreanu [a]

[a] Departamento de Análisis Matemático y Matemática Aplicada, Instituto de Matemática Interdisciplinar, Universidad Complutense de Madrid, Madrid, Spain

[b] Departamento de Matemática Aplicada, ICAI, Universidad Pontificia de Comillas, Madrid, Spain

ARTICLE INFO

Keywords:
Chemotaxis
Keller-Segel equations
Periodic solutions
Generalized finite difference method

ABSTRACT

In this work, we propose and analyze a mathematical model describing the interaction between a biological species and a lethal chemical substance, incorporating diffusion, negative chemotaxis, logistic growth, and toxicity effects. Motivated by the interaction between *E. coli* bacteria and hydrogen peroxide, the model accounts for a substance that simultaneously induces cell death and is self-produced by the population.

The dynamics are described by a system of nonlinear parabolic partial differential equations with an external supply of the substance. For constant supply rates, we study the local stability of spatially homogeneous steady states, showing that the balance between the logistic growth rate and the supply determines the linearized behavior of the system. When the supply is asymptotically time-periodic, we establish threshold conditions for the existence of periodic solutions through the analysis of an associated ODE system.

A numerical scheme based on the Generalized Finite Difference method is developed, and its convergence to the continuous solution is established. Numerical simulations are presented to validate the analytical results and to illustrate additional dynamical phenomena, including pattern formation.

1. Introduction

Chemotaxis is a biological phenomenon by which certain cells and organisms are able to direct their movement in response to chemical stimuli. Through specialized receptors, cells can detect spatial gradients in the concentration of chemical substances, resulting in motion toward higher concentrations, a behavior known as positive chemotaxis, or away from them, referred to as negative chemotaxis.

In this paper, we propose and analyze a system of two nonlinear parabolic partial differential equations modeling the dynamics of a bacterial population in competitive interaction with a lethal chemical substance —for instance an antibiotic— that can be self-produced by the bacteria.

It is assumed that bacterial motion is driven by random diffusion and negative chemotaxis in response to the chemical concentration. The population dynamics of the species are described by a logistic growth term, while the substance undergoes a degradation process in the form of an exponential decay. In addition, terms representing cell death and the production of the substance by the bacteria are incorporated, as well as an external supply of the substance, by means of a known source function f.

Such interactions occur in nature, for instance in the case of *E. coli* bacteria and hydrogen peroxide (H_2O_2). It has been shown that *E. coli* cells naturally produce between 10 and 15 μM of H_2O_2 per second [1,2]. Moreover, H_2O_2 acts as a chemorepellent (negative

* Corresponding author.
E-mail addresses: fedher01@ucm.es (F. Herrero-Hervás), negreanu@mat.ucm.es (M. Negreanu).

https://doi.org/10.1016/j.cnsns.2026.109645
Received 12 January 2025; Received in revised form 4 January 2026; Accepted 5 January 2026
Available online 6 January 2026

chemotaxis agent) [3] and, when its concentration can no longer be regulated by the cells' scavenging enzymes, can induce bacterial death [4] (see [5] for an analysis of the effects and killing rates of *E. coli* under different levels of exposure to H_2O_2).

Similar scenarios arise in bacterial species that naturally produce antibiotics, which can at times generate toxic effects against the cells themselves. For example, *Bacillus subtilis*, which produces bacilysin, may be susceptible to its effect under certain mutations, resulting in self-inhibition or cell death. A detailed description of how different antibiotic-producing organisms avoid such autotoxicity can be found in [6].

To describe these interactions, we model the process by the following initial-boundary value problem

$$\begin{cases} \dfrac{\partial u}{\partial t} = D_u \Delta u + \chi \nabla \cdot (u \nabla v) + ru\left(1 - \dfrac{u}{K}\right) - \delta u v, & x \in \Omega,\ t > 0, \\ \dfrac{\partial v}{\partial t} = D_v \Delta v + au - bv + f(x,t), & x \in \Omega,\ t > 0, \\ \dfrac{\partial u}{\partial \nu} = \dfrac{\partial v}{\partial \nu} = 0, & x \in \partial\Omega,\ t > 0, \\ u(x,0) = u_0(x), \quad v(x,0) = v_0(x), & x \in \Omega, \end{cases} \tag{1}$$

in a smooth and bounded domain $\Omega \subset \mathbb{R}^n$, where

- u and v denote the bacterial population density and the chemical concentration, respectively.
- $D_u > 0$, $D_v > 0$ and $\chi > 0$ are the diffusion coefficients of the bacteria and the substance, and the negative chemotaxis sensitivity, respectively.
- $r > 0$, $K > 0$ and $\delta > 0$ are the growth rate of the logistic model, its carrying capacity, and the death rate of the bacteria caused by the substance, respectively.
- $a \geq 0$, $b > 0$ and $f(x,t) \geq 0$ for all $x \in \Omega,\ t > 0$ are the self-production rate of the substance by the bacteria (in the case $a = 0$, the substance is not secreted by the bacteria, for instance when it represents and exogenous antibiotic), the degradation rate of the substance, and the known external supply of substance, respectively.
- $u_0(x)$ and $v_0(x)$ are the nonnegative initial values.

Historically, systems modeling chemotaxis were first introduced in the works of Keller and Segel [7,8] in the early 1970s, considering equations of the form

$$\begin{cases} \dfrac{\partial u}{\partial t} = D_1 \Delta u - \nabla \cdot (\chi u \nabla v) + f(u), & x \in \Omega,\ t > 0, \\ \tau \dfrac{\partial v}{\partial t} = D_2 \Delta v + au - bv, & x \in \Omega,\ t > 0, \end{cases} \tag{2}$$

for positive parameters $\chi,\ a,\ b$, a known function f representing the intrinsic dynamics of the species, and $\tau \in \{0, 1\}$, accounting for the possible difference in the timescales of u and v. System (2) was first introduced to model the aggregation process of a slime mold, although many variations have been studied over the years, corresponding to different biological scenarios (see the surveys [9–11]).

Competitive dynamics in the form of Lotka-Volterra terms have also been studied within different variations of chemotaxis models. The following system composed of two competitive species responding to one stimulus that induces positive chemotaxis has been extensively studied.

$$\begin{cases} \dfrac{\partial u}{\partial t} = D_1 \Delta u - \chi_1 \nabla \cdot (u \nabla w) + \mu_1 u(1 - u - a_1 v), & x \in \Omega,\ t > 0, \\ \dfrac{\partial v}{\partial t} = D_2 \Delta v - \chi_2 \nabla \cdot (u \nabla w) + \mu_2 v(1 - a_2 u - v), & x \in \Omega,\ t > 0, \\ \tau \dfrac{\partial w}{\partial t} = D_3 \Delta w - \gamma w + \alpha u + \beta v, & x \in \Omega,\ t > 0, \end{cases} \tag{3}$$

where in this case, u and v denote the population densities of the two species, while w is the concentration of the chemical substance. The parabolic case (corresponding to $\tau = 1$) was analyzed by Bai and Winkler in [12], where the global existence of solutions for $n \leq 2$ was proven under certain restrictions for μ_1 and μ_2. The large time convergence of solutions to its spatially homogeneous steady states was also studied. These results were improved later in [13], with lighter restrictions on μ_1 and μ_2. The higher dimensional case was analyzed in [14]

Respectively, the elliptic case (for $\tau = 0$) has been studied in [15] for the weakly competitive case ($0 < a_1, a_2 < 1$) with similar restrictions for μ_1, μ_2 and χ_1, χ_2 leading to the convergence to its spatially homogeneous steady states. In [16] a competitive exclusion result is obtained.

In this paper, we consider a single species, with the competitive term appearing only in the first equation of (1), representing the cell death induced by the chemical.

After introducing the rescaled variables

$$\tilde{u} = \frac{u}{K},\ \tilde{v} = \frac{\delta K}{b} v,\ \tilde{x} = \sqrt{\frac{b}{D_v}} x,\ \tilde{t} = bt,$$

and the dimensionless parameters

$$D = \frac{D_u}{D_v},\ \tilde{\chi} = \frac{b\chi}{\delta K D_v},\ \tilde{r} = \frac{r}{b},\ \tilde{a} = \frac{a\delta K^2}{b^2},\ \tilde{f} = \frac{\delta K}{b^2} f,$$

the system can be rewritten as follows. For simplicity, the tildes have been dropped.

$$\begin{cases} \dfrac{\partial u}{\partial t} = D\Delta u + \chi\nabla\cdot(u\nabla v) + ru(1-u) - uv, & x\in\Omega,\ t>0,\\ \dfrac{\partial v}{\partial t} = \Delta v + au - v + f(x,t), & x\in\Omega,\ t>0,\\ \dfrac{\partial u}{\partial \nu} = \dfrac{\partial v}{\partial \nu} = 0, & x\in\partial\Omega,\ t>0,\\ u(x,0) = u_0(x), \quad v(x,0) = v_0(x), & x\in\Omega. \end{cases} \tag{4}$$

Throughout this paper, we study the local stability of the spatially homogeneous steady states of system (4) when f is a constant supply, as well as the periodicity of solutions for choices of f with a persisting time-periodic behavior.

For a constant f, system (4) admits two spatially homogeneous steady states, given by

$$(0,f), \quad (u_*,v_*) := \left(\frac{r-f}{r+a}, \frac{r(f+a)}{r+a}\right).$$

The nontrivial state (u_*,v_*) is only biologically relevant if $r>f$, that is, when the bacterial growth rate is greater than the external supply of the substance. Conversely, if $r<f$, the only nonnegative equilibrium is given by $(0,f)$. The linearized dynamics and local stability of these solutions are studied in Section 2.

The analysis of system (4) under a supply f with persisting periodic behavior is carried out in Section 3. Specifically, we assume that f is asymptotically periodic, in the sense that there exists a time periodic function $\hat{f}:[0,+\infty)\to\mathbb{R}$ depending only on t, such that

$$\lim_{t\to+\infty}\sup_{x\in\Omega}|f(x,t)-\hat{f}(t)| = 0.$$

Under this assumption, it has recently been proven in [17] that, with additional hypotheses, the solution (u,v) of system (4) converges in time to those of the associated ODE system

$$\begin{cases} \dfrac{d\tilde{u}}{dt} = r\tilde{u}(1-\tilde{u}) - \tilde{u}\tilde{v}, & t>0,\\ \dfrac{d\tilde{v}}{dt} = a\tilde{u} - \tilde{v} + \hat{f}(t), & t>0, \end{cases} \tag{5}$$

with initial values

$$\tilde{u}(0) = \frac{1}{|\Omega|}\int_\Omega u(x,0)\,dx, \quad \tilde{v}(0) = \frac{1}{|\Omega|}\int_\Omega v(x,0)\,dx. \tag{6}$$

However, it remains unclear under which conditions do $(\tilde{u},\tilde{v})$ inherit the periodicity of $\hat{f}$. Here, we provide a partial answer, proving that in the case $a=0$ there exists a unique positive periodic solution if a threshold value for r is satisfied. Moreover, when $a>0$, numerical experiments performed also allow us to obtain such periodic solutions under particular choices of r. In these cases, a numerical resolution of system (4) shows that, as expected, the periodic behavior of the solutions to the ODE system (5) is inherited by the PDE system, with solutions (u,v) converging uniformly in time to $(\tilde{u},\tilde{v})$.

For such numerical study, we employ the Generalized Finite Difference (GFD) method, a meshless approach that has been successfully applied to a wide range of nonlinear problems. Precisely within the context of chemotaxis systems, the authors in [18–22] study various extensions of the Keller-Segel model, including parabolic-parabolic, parabolic-elliptic and parabolic-ODE problems.

In our case, after a preliminary introduction of the method in Section 4, we derive conditions for the convergence of an explicit scheme in Section 5, which allows us to compute numerical solutions to system (4). Various simulation results are included in Section 6 to illustrate the cases studied analytically throughout the previous sections, including the local stability of the steady states and the eventual periodicity of solutions, as well as a brief subsection regarding pattern formation in the system. Lastly, the conclusions are collected in Section 7.

2. Linearized dynamics and local stability

To begin the analysis of system (4), we study the local stability of its spatially homogeneous steady states. While global existence and boundedness of solutions to system (4), are analyzed in [17], the present work focuses on the dynamics near homogeneous equilibria. With the aim of numerically exploring the properties of the system, this local stability analysis serves as a basis for the expected behavior of solutions.

To this end, the spatially homogeneous steady states of system (4) are obtained by solving

$$\begin{cases} 0 = ru\left(1-u-\dfrac{v}{r}\right),\\ 0 = au - v + f(x,t). \end{cases}$$

Such solutions can only exist for a constant source term $f(x,t)\equiv f$, yielding the two equilibria

$$(0,f), \quad (u_*,v_*) := \left(\frac{r-f}{r+a}, \frac{r(f+a)}{r+a}\right). \tag{7}$$

From a biological perspective, we require that both u and v are nonnegative, and thus (u_*, v_*) is only meaningful if $r > f$, that is, when the logistic growth rate of the population is greater than the external supply of the substance.

To assess the local stability of the steady states (7), we make use of the principle of linearized stability for quasilinear parabolic problems, [23]. As the analysis is standard (see for instance [24] for a similar derivation with full details) we only outline the main steps. Letting $(\bar{u}, \bar{v})$ denote any of the previous spatially homogeneous steady states, we consider perturbed solutions of the form

$$u = \bar{u} + \varepsilon\phi, \quad v = \bar{v} + \varepsilon\eta \tag{8}$$

for $0 < \varepsilon \ll 1$. Substituting into system (4) and neglecting the terms of order ε^2, the following linearized system is obtained

$$\begin{cases} \dfrac{\partial \phi}{\partial t} = D\Delta\phi + \chi\bar{u}\Delta\eta + [(1-2\bar{u})r - \bar{v}]\phi - \bar{u}\eta, & x \in \Omega,\ t > 0, \\ \dfrac{\partial \eta}{\partial t} = \Delta\eta + a\phi - \eta, & x \in \Omega,\ t > 0, \end{cases} \tag{9}$$

together with Neumann homogeneous boundary conditions and their respective initial values. The local stability analysis of the linearized system (9) reduces to studying the eigenvalues of $\boldsymbol{A}_n := -\lambda_n \boldsymbol{D} + \boldsymbol{J}$ for all $n \in \{0, 1, 2, \dots\}$, where

$$\boldsymbol{D} = \begin{pmatrix} D & \chi\bar{u} \\ 0 & 1 \end{pmatrix}, \quad \boldsymbol{J} = \begin{pmatrix} (1-2\bar{u})r - \bar{v} & -\bar{u} \\ a & -1 \end{pmatrix},$$

and $\{\lambda_n\}_{n\in\mathbb{N}\cup\{0\}}$ is the sequence of eigenvalues

$$0 = \lambda_0 < \lambda_1 \le \lambda_2 \le \dots, \quad \text{with } \lim_{n\to\infty} \lambda_n = +\infty \tag{10}$$

of the operator $-\Delta$ over Ω with Neumann homogeneous boundary conditions.

We recall that a given spatially homogeneous steady state $(\bar{u}, \bar{v})$ is locally asymptotically stable if and only if all the eigenvalues of $\boldsymbol{A}_n$ have negative real part for all $n \in \mathbb{N} \cup \{0\} =: \mathbb{N}_0$. On the contrary, if there exists n such that $\boldsymbol{A}_n$ has at least one eigenvalue with positive real part, then $(\bar{u}, \bar{v})$ is unstable. The computations for the first state, $(\bar{u}, \bar{v}) = (0, f)$, yield

$$\boldsymbol{A}_n = \begin{pmatrix} -\lambda_n D + r - f & 0 \\ a & -\lambda_n - 1 \end{pmatrix},$$

whose eigenvalues are trivially given by $\mu_{n_1} := -\lambda_n D + r - f$ and $\mu_{n_2} := -\lambda_n - 1$. It is then clear from (10) that $\mu_{n_2} < 0$ for all $n \in \mathbb{N}_0$. With respect to μ_{n_1}, as $\lambda_0 = 0$, it follows that $\mu_{0_1} < 0$ if and only if $r < f$. For $n \ge 1$, as the sequence λ_n is increasing, $\mu_{n_1} < \mu_{0_1}$. We therefore conclude that $(0, f)$ is locally asymptotically stable if and only if $r < f$, while for $r > f$, the point is unstable.

Similarly, for $(\bar{u}, \bar{v}) = (u_*, v_*) = \left(\dfrac{r-f}{r+a}, \dfrac{r(f+a)}{r+a}\right)$, $\boldsymbol{A}_n$ is given by

$$\boldsymbol{A}_n = \begin{pmatrix} -\lambda_n D + \dfrac{r(f-r)}{r+a} & \dfrac{f-r}{r+a}(\lambda_n\chi + 1) \\ a & -\lambda_n - 1 \end{pmatrix}$$

Denoting again by μ_{n_1}, μ_{n_2} the two eigenvalues of $\boldsymbol{A}_n$ for every $n \in \mathbb{N}_0$, as $\boldsymbol{A}_n$ is a 2×2 matrix, we have

$$\begin{aligned} \operatorname{tr}(\boldsymbol{A}_n) &= \mu_{n_1} + \mu_{n_2} = -\lambda_n D + \frac{r(f-r)}{r+a} - \lambda_n - 1, \\ \det(\boldsymbol{A}_n) &= \mu_{n_1}\mu_{n_2} = -(\lambda_n + 1)\left(-\lambda_n D + \frac{r(f-r)}{r+a}\right) - a \cdot \frac{f-r}{r+a} \cdot (\lambda_n\chi + 1). \end{aligned}$$

Given that, for biological relevance, we are only interested in the case $r > f$, clearly $\mu_{n_1} + \mu_{n_2} < 0$ and $\mu_{n_1}\mu_{n_2} > 0$ for all $n \in \mathbb{N}_0$, resulting in the local asymptotic stability of the state (u_*, v_*).

As a consequence, we conclude that

- If $r < f$, the only nonnegative spatially homogeneous steady state is $(0, f)$, which is locally asymptotically stable.
- If $r > f$, both spatially homogeneous steady states, $(0, f)$ and (u_*, v_*), are biologically meaningful. In this case, $(0, f)$ is unstable, whereas (u_*, v_*) is locally asymptotically stable.

From a biological point of view, if $r < f$ —this is, if the constant external supply of the substance exceeds the logistic growth rate of the bacteria— then $(0, f)$ is the only existing spatially homogeneous steady state, and is locally asymptotically stable. Consequently, sufficiently small perturbations around this equilibrium decay over time, as the intrinsic bacterial growth is not large enough to compensate the death term $-uv$, due to the high concentration of v that originate from the large supply rate f.

On the contrary, if $r > f$, the state $(0, f)$ is unstable, as the external supply is smaller than the logistic growth rate, fostering the bacterial proliferation. The other spatially homogeneous steady state, (u_*, v_*) of coexistence of the bacteria and the species, is locally asymptotically stable. In this case, despite the growth being greater than the supply, both u and v are large enough for $-uv$ to significantly counteract it.

We remark that the local stability is independent of the remaining parameters, D, χ and a, and thus the linearized dynamics of the system are governed solely by the balance between the constant supply rate f and the logistic growth rate r.

3. Periodic solutions

Next, we analyze the existence of periodic solutions to system (4) under a source f with asymptotic periodic behavior, that is, satisfying

$$\lim_{t\to+\infty}\sup_{x\in\Omega}|f(x,t)-\hat{f}(t)|=0,$$

for a certain time-periodic function $\hat{f}$ of period $T>0$. This assumption is standard and has been employed in other similar works such as [25,26].

As stated in the introduction, it has been proven in [17] that under suitable hypotheses, the solution (u,v) of system (4) converges in time to $(\tilde{u},\tilde{v})$, the solution of the associated ODE system (5) with initial values given by the spatial averages of $u(x,0)$ and $v(x,0)$, as stated in (6). Consequently, periodic behavior in the full PDE model can be characterized by periodicity in the ODE dynamics. The aim of this section is to therefore identify conditions under which $(\tilde{u},\tilde{v})$ inherit the periodicity of $\hat{f}$, which then lead to periodicity of (u,v).

We first consider the case $a=0$, corresponding to a situation in which the substance is not produced by the bacteria. In this case, the associated ODE system reduces to

$$\begin{cases}\dfrac{d\tilde{u}}{dt}=r\tilde{u}(1-\tilde{u})-\tilde{u}\tilde{v}, & t>0,\\[2mm] \dfrac{d\tilde{v}}{dt}=-\tilde{v}+\hat{f}(t), & t>0,\end{cases}\tag{11}$$

where the second equation is now linear and uncoupled, allowing for an explicit characterization of its periodic solutions. Solving for $\tilde{v}$, one obtains

$$\tilde{v}(t)=e^{-t}\left[\tilde{v}_0+\int_0^t\hat{f}(s)e^s\,ds\right].\tag{12}$$

Given that $\hat{f}$ is $T-$periodic, a necessary and sufficient condition for $\tilde{v}$ to be $T-$periodic as well is that $\tilde{v}(T)=\tilde{v}_0$. Thus, to yield this condition, it follows from (12) that v_0 must satisfy

$$\tilde{v}_0=\frac{1}{e^T-1}\int_0^T\hat{f}(s)e^s\,ds.\tag{13}$$

A similar analysis can be done for $\tilde{u}$, noting that, for a known $\tilde{v}$, it becomes a Bernoulli equation, which can again be explicitly solved. By considering $\tilde{w}=\tilde{u}^{-1}$, a linear equation in $\tilde{w}$ is retrieved, whose solution is given by

$$\tilde{w}(t)=e^{-\int_0^t(r-\tilde{v}(s))\,ds}\left[\frac{1}{\tilde{u}_0}+\int_0^t\left(r\,e^{\int_0^s(r-\tilde{v}(\tau))\,d\tau}\right)ds\right].\tag{14}$$

Thus, assuming $\tilde{v}$ is periodic, provided $\tilde{v}_0$ satisfies (13), the periodicity of $\tilde{u}$ is ensured if and only if $\tilde{u}(T)=\tilde{u}_0$ or equivalently $\tilde{w}(T)=\tilde{w}_0:=1/\tilde{u}_0$. This leads to

$$\tilde{u}_0=\frac{e^{\int_0^T(r-\tilde{v}(s))\,ds}-1}{\displaystyle\int_0^T\left(r\,e^{\int_0^s(r-\tilde{v}(\tau))\,d\tau}\right)ds}.\tag{15}$$

Hence, the solution $(\tilde{u},\tilde{v})$ of (11) is $T-$periodic if and only if the initial values $(\tilde{u}_0,\tilde{v}_0)$ satisfy (13) and (15).

It is important to emphasize that $(\tilde{u}_0,\tilde{v}_0)$ are not arbitrary, as they are uniquely determined by (6) as the spatial averages of the initial bacterial and chemical distributions $u(x,0)$ and $v(x,0)$. As a result, the periodicity conditions (13) and (15) translate into constraints on the admissible initial data of the full PDE system (4).

An important bound can be derived from (15). For biological relevance, only positive solutions are considered. In particular, the positivity of $\tilde{u}_0$, requires

$$e^{\int_0^T(r-\tilde{v}(s))\,ds}-1>0,$$

or equivalently

$$r>\frac{1}{T}\int_0^T\tilde{v}(s)\,ds.$$

This yields the threshold

$$r_{\min}=\frac{1}{T}\int_0^T\tilde{v}(s)\,ds.\tag{16}$$

If $r > r_{\min}$ and $(\tilde{u}_0, \tilde{v}_0)$ are taken according to (15) and (13), then the unique solution $(\tilde{u}, \tilde{v})$ of system (11) is positive and $T-$periodic. Moreover, this solution is such that for any other positive choice of initial values, the associated solution converges in time to it. On the contrary, if $r \leq r_{\min}$, no solution with such properties exists, and for any pair of initial values, $\tilde{u} \to 0$ as $t \to \infty$.

Notice that in fact the threshold (16) acts as bound for r with respect to the choice of $\hat{f}$, given that $\tilde{v}$ is independent from r. Directly substituting the expression for $\tilde{v}$ given in (12) into (16) and integrating by parts using the value of $\tilde{v}_0$ from (13), yields

$$r_{\min} = \frac{1}{T}\int_0^T \hat{f}(s)\, ds. \tag{17}$$

Thus, for a given $\hat{f}$, only a species with a logistic growth rate above $r_{\min}$ can sustain a periodically oscillatory regime. This result highlights a threshold phenomenon analogous to that observed in the local stability analysis for constant sources. In this case, the existence of periodic solutions of the associated ODE system is governed by condition (17), involving solely the logistic growth rate r and the average value of $\hat{f}$ over $[0, T]$. This is similar to the result obtained for a constant source satisfying $r > f$, for which the coexistence equilibrium (u_*, v_*) was locally asymptotically stable.

Biologically, these dynamics —either periodicity or local stability— arise only when the logistic growth rate of the species is sufficiently large compared to the external supply, either in terms of its average over one period or directly its value in the case of a constant supply. Conversely, when the supply exceeds the logistic growth rate, the bacterial population is driven to extinction in both settings.

For the case $a > 0$, corresponding to a substance self-produced by the bacteria, the existence and properties of periodic solutions to the associated ODE system have so far been investigated only at the numerical level; see Section 6.2. A complete analytical characterization of this regime still remains open due to the nonlinear coupling of the equations.

4. Preliminaries for the numerical method

In order to numerically solve system (4), we employ the Generalized Finite Difference (GFD) method. This meshless approach, developed as an extension of the classical Finite Difference method, allows for a set of nodes that may be irregularly distributed over the domain —thus avoiding any geometrical restrictions— on which an approximation of the solution is computed. A numerical scheme is constructed by obtaining finite difference approximation formulae for the partial derivatives. Below, we outline the basics of the method before presenting in Section 5 the numerical scheme obtained.

To do so, let Ω be the considered domain in $\mathbb{R}^m$ and $M = \{\boldsymbol{x}_1, \boldsymbol{x}_2, \dots \boldsymbol{x}_N\}$ a discretization of such domain, where we seek to approximate the solution of a given equation. For ease of notation and without loss of generality, we consider dimension $m = 2$ and we fix an interior node of M which we denote by $\boldsymbol{x}_0$. In a neighborhood of $\boldsymbol{x}_0$, we select a subset $V = \{\boldsymbol{x}_1, \boldsymbol{x}_2, \dots, \boldsymbol{x}_s\} \subset M \setminus \{\boldsymbol{x}_0\}$, of s nodes, which constitute what is known as an E_s-star. There exist different geometrical criteria, such as distance-based, quadrant or octant criteria (see [27]) to select the s nodes preventing ill-behaved stars.

In order to obtain the finite difference approximations for the derivatives of an arbitrary function $f(\boldsymbol{x}, t)$ at $\boldsymbol{x}_0 := (x_0, y_0)$, we consider its truncated second-order Taylor expansion. Denoting as usual by F_i^n the sought approximation of $f(\boldsymbol{x}_i, n\Delta t)$ (although we omit the time dependence n for the moment) we obtain

$$F_i \approx F_0 + (\boldsymbol{x}_i - \boldsymbol{x}_0)\nabla F_0 + \frac{1}{2}(\boldsymbol{x}_i - \boldsymbol{x}_0)^T H_{F_0}(\boldsymbol{x}_i - \boldsymbol{x}_0). \tag{18}$$

We next define the vectors

$$\boldsymbol{d} := \left(\frac{\partial F_0}{\partial x}, \frac{\partial F_0}{\partial y}, \frac{\partial^2 F_0}{\partial x^2}, \frac{\partial^2 F_0}{\partial y^2}, \frac{\partial^2 F_0}{\partial x \partial y}\right)^T, \quad \boldsymbol{c}_i = \left(h_i, k_i, \frac{h_i^2}{2}, \frac{k_i^2}{2}, h_i k_i\right)^T,$$

where $\boldsymbol{d}$ contains the partial derivatives of that we seek to approximate, and $\boldsymbol{c}_i$ is defined for each node $\boldsymbol{x}_i := (x_i, y_i) \in V$, where $h_i := x_i - x_0$ and $k_i := y_i - y_0$.

Based on the approximation (18), we define the following weighted sum of the quadratic errors made when approximating each F_i, for $i \in \{1, \dots, s\}$, by the above Taylor expansion centered on $\boldsymbol{x}_0$.

$$B(\boldsymbol{d}) = \sum_{i=1}^{s} w_i^2 (F_0 - F_i + \boldsymbol{c}_i^T \boldsymbol{d})^2 + \mathcal{O}(h_i^2, k_i^2).$$

The weights $w_i = w(h_i, k_i)$ are positive symmetric functions that decrease in magnitude as the distance to the center $\boldsymbol{x}_0$ increases, as defined in Lancaster and Salkauskas [28]. Some commonly used weights are inverse powers (dist^{-4} or dist^{-6}) or exponential weights, $e^{-\text{dist}^2}$ (more details can be found in [29]). To obtain the best second-order least-squares approximation of the partial derivatives of f, B is minimized with respect to $\boldsymbol{d}$, yielding the following linear system of equations

$$\sum_{i=1}^{s} w_i^2 \boldsymbol{c}_i \boldsymbol{c}_i^T \boldsymbol{d} = -\sum_{i=1}^{s} w_i^2 (F_0 - F_i)\boldsymbol{c}_i.$$

The coefficient matrix is $\boldsymbol{A} := \sum_{i=1}^{s} w_i^2 \boldsymbol{c}_i \boldsymbol{c}_i^T \in \mathcal{M}_{5\times 5}(\mathbb{R})$, which can be expressed as

$$\boldsymbol{A} = \begin{pmatrix} h_1 & h_2 & \cdots & h_s \\ k_1 & k_2 & \cdots & k_s \\ \frac{h_1^2}{2} & \frac{h_2^2}{2} & \cdots & \frac{h_s^2}{2} \\ \frac{k_1^2}{2} & \frac{k_2^2}{2} & \cdots & \frac{k_s^2}{2} \\ h_1k_1 & h_2k_2 & \cdots & h_sk_s \end{pmatrix} \cdot \begin{pmatrix} w_1^2 & & & \\ & w_2^2 & & \\ & & \ddots & \\ & & & w_s^2 \end{pmatrix} \cdot \begin{pmatrix} h_1 & k_1 & \frac{h_1^2}{2} & \frac{k_1^2}{2} & h_1k_1 \\ h_2 & k_2 & \frac{h_2^2}{2} & \frac{k_2^2}{2} & h_2k_2 \\ \vdots & \vdots & \vdots & \vdots & \vdots \\ h_s & k_s & \frac{h_s^2}{2} & \frac{k_s^2}{2} & h_sk_s \end{pmatrix} \tag{19}$$

Properties of $\boldsymbol{A}$ are well-known, and can be consulted in [29]. In particular, it is positive definite and, therefore,

$$\boldsymbol{d} = -F_0 \sum_{i=1}^{s} w_i^2 \boldsymbol{A}^{-1}\boldsymbol{c}_i + \sum_{i=1}^{s} F_i w_i^2 \boldsymbol{A}^{-1}\boldsymbol{c}_i + \mathcal{O}(h^2, k^2),$$

where we denote by

$$h := \max_{i\in\{1,\dots s\}} h_i, \quad k := \max_{i\in\{1,\dots s\}} k_i.$$

In addition, for simplicity, we write

$$\boldsymbol{m}_i = w_i^2 \boldsymbol{A}^{-1}\boldsymbol{c}_i, \quad \boldsymbol{m}_0 = \sum_{i=1}^{s} \boldsymbol{m}_i,$$

and denote $\boldsymbol{m}_0 =: (m_{01}, m_{02}, m_{03}, m_{04}, m_{05})^T$ (and similarly for $\boldsymbol{m}_i$). This allows us to express the partial derivatives of the function f as a linear combination of its values over the points of the star, yielding

$$\begin{cases} \dfrac{\partial F(\mathbf{x}_0, n\Delta t)}{\partial x} = -m_{01}F_0^n + \sum_{i=1}^{s} m_{i1}F_i^n + \mathcal{O}(h^2, k^2), \\ \dfrac{\partial F(\mathbf{x}_0, n\Delta t)}{\partial y} = -m_{02}F_0^n + \sum_{i=1}^{s} m_{i2}F_i^n + \mathcal{O}(h^2, k^2), \\ \dfrac{\partial^2 F(\mathbf{x}_0, n\Delta t)}{\partial x^2} + \dfrac{\partial^2 F(\mathbf{x}_0, n\Delta t)}{\partial y^2} = -(m_{03}+m_{04})F_0^n + \sum_{i=1}^{s}(m_{i3}+m_{i4})F_i^n \\ \qquad\qquad =: -m_{00}F_0 + \sum_{i=1}^{s} m_{i0}F_i + \mathcal{O}(h^2, k^2). \end{cases} \tag{20}$$

For the time derivative, in order to obtain an explicit scheme, its approximation is computed through a classical first-order forward difference formula

$$\frac{\partial F(\mathbf{x}_0, n\Delta t)}{\partial t} = \frac{F_0^{n+1} - F_0^n}{\Delta t} + \mathcal{O}(\Delta t), \tag{21}$$

at evenly spaced time points. Thus, for a given second-order parabolic equation, substituting the finite difference approximations (20) and (21), yields an explicit GFD scheme. For system (4), we present the scheme in the next section, proving its convergence to the continuous solution.

5. Numerical scheme and convergence

Having developed the fundamentals of the GFD method in the previous section, we now turn to system (4) and obtain an explicit scheme for its numerical approximation.

Substituting the second-order finite difference formulae (20) for the spatial derivative and the first-order forward difference (21) into system (4) provides the following explicit GFD scheme

$$\begin{cases} u_0^{n+1} = u_0^n + \Delta t\Big[D\Big(-m_{00}u_0^n + \sum_{i=1}^{s} m_{0i}u_i^n\Big) - \chi u_0^n\Big(-m_{00}v_0^n + \sum_{i=1}^{s} m_{0i}v_i^n\Big)\Big] \\ \qquad +\chi\Delta t\Big(-m_{01}u_0^n + \sum_{i=1}^{s} m_{i1}u_i^n\Big)\Big(-m_{01}v_0^n + \sum_{i=1}^{s} m_{i1}v_i^n\Big) \\ \qquad +\chi\Delta t\Big(-m_{02}u_0^n + \sum_{i=1}^{s} m_{i2}u_i^n\Big)\Big(-m_{02}v_0^n + \sum_{i=1}^{s} m_{i2}v_i^n\Big) \\ \qquad +\Delta t\cdot ru_0^n\big(1-u_0^n\big) - \Delta t\cdot u_0^n v_0^n, \\ v_0^{n+1} = v_0^n\Big[1 - \Delta t\cdot(1+m_{00})\Big] + \Delta t\cdot au_0^n + \Delta t\sum_{i=1}^{s} m_{0i}v_i^n + f_0^n, \end{cases} \tag{22}$$

initiated at $t = 0$ with the initial values $u(x, 0)$ and $v(x, 0)$. The explicit nature of scheme (22) requires, as usual, the determination of an upper bound for the time step Δt that guarantees its convergence. To do so, we first define the following quantities for each inner node

$$
\begin{aligned}
A_1 :=& \Big|\chi V_0^n\big(m_{01}^2+m_{02}^2\big)-\chi\Big(m_{01}\sum_{i=1}^{s}m_{i1}V_i^n+m_{02}\sum_{i=1}^{s}m_{i2}V_i^n\Big)\\
&-(\chi-\mu)(u_0^n+U_0^n)+\chi V_0^n-\mu\big(1+f(x_0,y_0,n\Delta t)\big)\Big|\\
&+\chi v_0^n\Big(|m_{01}|\sum_{i=1}^{s}|m_{i1}|+|m_{02}|\sum_{i=1}^{s}|m_{i2}|\Big)\\
&+\chi\Big(\Big|\sum_{i=1}^{s}m_{i1}V_i^n\Big|\sum_{i=1}^{s}|m_{i1}|+\Big|\sum_{i=1}^{s}m_{i2}V_i^n\Big|\sum_{i=1}^{s}|m_{i2}|\Big),
\end{aligned}
\tag{23}
$$

$$
\begin{aligned}
B_1 :=& \Big|-\chi u_0^n(m_{01}^2+m_{02}^2+1)+\chi\Big(m_{01}\sum_{i=1}^{s}m_{i1}u_i^n+m_{02}\sum_{i=1}^{s}m_{i2}u_i^n\Big)\Big|\\
&+\chi U_0^n\Big(|m_{01}|\sum_{i=1}^{s}|m_{i1}|+|m_{02}|\sum_{i=1}^{s}|m_{i2}|\Big)\\
&+\chi\Big(\Big|\sum_{i=1}^{s}m_{i1}U_i^n\Big|\sum_{i=1}^{s}|m_{i1}|+\Big|\sum_{i=1}^{s}m_{i2}U_i^n\Big|\sum_{i=1}^{s}|m_{i2}|\Big),
\end{aligned}
\tag{24}
$$

which are finite constants as a consequence of the uniform $L^\infty(\Omega)$ bounds of the solution of system (4).

Theorem 1. *Let $U, V \in C^4(\Omega\times(0,\infty))$ be the exact solution of (1). Then, the GFD explicit scheme (22) is convergent if for every inner node*

$$
\Delta t < \min\left\{\frac{2}{Dm_{00}+D\sum_{i=1}^{s}|m_{i0}|+A_1+B_1},\frac{2}{1+m_{00}+\sum_{i=1}^{s}|m_{i0}|+a}\right\},
\tag{25}
$$

for the values of A_1 and B_1 given in (23) and (24).

Proof of Theorem 1

Let u_j^n denote the numerical approximation of u at node j and time $n\Delta t$ (similarly for v_j^n), and let U_j^n and V_j^n be the exact solutions evaluated at the same node and time. We define the discrete errors by

$$
\tilde{u}_j^n := u_j^n - U_j^n, \quad \tilde{v}_j^n := v_j^n - V_j^n
$$

Beginning by the u equation, subtracting the numerical scheme (22) from the exact solution yields the following expression

$$
\begin{aligned}
\tilde{u}_0^{n+1} =& \tilde{u}_0^n + D\Delta t\Big(-m_{00}\tilde{u}_0^n+\sum_{i=1}^{s}m_{i0}\tilde{u}_i^n\Big)\\
&+\chi\Delta t\Big[\Big(-m_{01}u_0^n+\sum_{i=1}^{s}m_{i1}u_i^n\Big)\Big(-m_{01}v_0^n+\sum_{i=1}^{s}m_{i1}v_i^n\Big)\\
&\quad-\Big(-m_{01}U_0^n+\sum_{i=1}^{s}m_{i1}U_i^n\Big)\Big(-m_{01}V_0^n+\sum_{i=1}^{s}m_{i1}V_i^n\Big)\Big]\\
&+\chi\Delta t\Big[\Big(-m_{02}u_0^n+\sum_{i=1}^{s}m_{i2}u_i^n\Big)\Big(-m_{02}v_0^n+\sum_{i=1}^{s}m_{i2}v_i^n\Big)\\
&\quad-\Big(-m_{02}U_0^n+\sum_{i=1}^{s}m_{i2}U_i^n\Big)\Big(-m_{02}V_0^n+\sum_{i=1}^{s}m_{i2}V_i^n\Big)\Big]\\
&-\chi\Delta t\Big[m_{00}(\tilde{u}_0^n v_0^n+U_0^n\tilde{v}_0^n)-\Big(\tilde{u}_0^n\sum_{i=1}^{s}m_{i0}v_i^n+U_0^n\sum_{i=1}^{s}m_{i0}\tilde{v}_i^n\Big)\Big]\\
&-\Delta t\Big[r\tilde{u}_0^n[1-(u_0^n+U_0^n)]-\tilde{u}_0^n v_0^n-U_0^n\tilde{v}_0^n\Big]+\mathcal{O}(\Delta t,h^2,k^2).
\end{aligned}
\tag{26}
$$

By expanding the products and regrouping terms, we obtain

$$\begin{aligned}
\tilde{u}_0^{n+1} = \tilde{u}_0^n\Big[1 &- \Delta t\Big(Dm_{00} + \chi m_{01}^2 V_0^n + \chi m_{02}^2 V_0^n\Big)\\
&- \Delta t\chi\Big(m_{01}\sum_{i=1}^{s} m_{i1}v_i^n + m_{02}\sum_{i=1}^{s} m_{i2}v_i^n + \sum_{i=1}^{s} m_{i0}v_i^n\Big)\\
&- \Delta t\Big(\chi m_{00}v_0^n - r[1-(u_0^n+U_0^n)] - v_0^n\Big)\Big]\\
&+ \Delta t\Big[D\sum_{i=1}^{s} m_{i0}\tilde{u}_i^n - \chi m_{01}V_0^n\sum_{i=1}^{s} m_{i1}\tilde{u}_i^n - \chi m_{02}V_0^n\sum_{i=1}^{s} m_{i2}\tilde{u}_i^n\\
&+ \Big(\chi\sum_{i=1}^{s} m_{i1}v_i^n\Big)\sum_{i=1}^{s} m_{i1}\tilde{u}_i^n + \Big(\chi\sum_{i=1}^{s} m_{i2}v_i^n\Big)\sum_{i=1}^{s} m_{i2}\tilde{u}_i^n\Big]\\
&+ \Delta t\ \tilde{v}_0^n\Big[\chi\Big(m_{01}^2+m_{02}^2)U_0^n - m_{01}\sum_{i=1}^{s} m_{i1}u_i^n\Big)\\
&- \chi m_{02}\sum_{i=1}^{s} m_{i2}u_i^n - \chi m_{00}U_0^n - U_0^n\Big]\\
&+ \Delta t\Big[-\chi m_{01}U_0^n\sum_{i=1}^{s} m_{i1}\tilde{v}_i^n - \chi m_{02}U_0^n\sum_{i=1}^{s} m_{i2}\tilde{v}_i^n\\
&+ \chi\Big(\sum_{i=1}^{s} m_{i1}U_i^n\Big)\sum_{i=1}^{s} m_{i1}\tilde{v}_i^n + \chi\Big(\sum_{i=1}^{s} m_{i2}U_i^n\Big)\sum_{i=1}^{s} m_{i2}\tilde{v}_i^n\Big]\\
&+ \mathcal{O}(\Delta t, h^2, k^2).
\end{aligned} \tag{27}$$

Next, we define $\tilde{u}^n := \max_{i\in\{0,\dots,s\}} |\tilde{u}_i^n|$, and $\tilde{v}^n := \max_{i\in\{0,\dots,s\}} |\tilde{v}_i^n|$, rewriting (27) as

$$\begin{aligned}
\tilde{u}^{n+1} \le \tilde{u}^n\Bigg[&\Bigg|1 - \Delta t\Big[Dm_{00} - \chi m_{01}^2 V_0^n - \chi m_{02}^2 V_0^n + \chi m_{00}v_0^n + v_0^n\\
&+ r[1-(u_0^n+U_0^n)] + \chi\Big(m_{01}\sum_{i=1}^{s} m_{i1}v_i^n + m_{02}\sum_{i=1}^{s} m_{i2}v_i^n - \sum_{i=1}^{s} m_{i0}v_i^n\Big)\Big]\Bigg|\\
&+ \Delta t\ D\sum_{i=1}^{s}|m_{i0}| + \chi\Big|m_{01}V_0^n\sum_{i=1}^{s} m_{i1}\Big| + \chi\Big|m_{02}V_0^n\sum_{i=1}^{s} m_{i2}\Big|\\
&+ \Big|\chi\sum_{i=1}^{s} m_{i1}v_i^n\Big|\sum_{i=1}^{s}|m_{i1}| + \Big|\chi\sum_{i=1}^{s} m_{i2}v_i^n\Big|\sum_{i=1}^{s}|m_{i2}|\Bigg]\\
+ \tilde{v}^n\Delta t\Bigg[&\Bigg|\chi\Big((m_{01}^2+m_{02}^2)U_0^n - m_{01}\sum_{i=1}^{s} m_{i1}u_i^n - m_{02}\sum_{i=1}^{s} m_{i2}u_i^n - m_{00}U_0^n\Big) - U_0^n\Bigg|\\
&+ \chi\Big(\Big|m_{01}U_0^n\sum_{i=1}^{s} m_{i1}\Big| + \Big|m_{02}U_0^n\sum_{i=1}^{s} m_{i2}\Big| + \Big|\sum_{i=1}^{s} m_{i1}U_i^n\Big|\sum_{i=1}^{s}|m_{i1}|\Big)\\
&+ \chi\Big|\sum_{i=1}^{s} m_{i2}U_i^n\Big|\sum_{i=1}^{s}|m_{i2}|\Bigg] + \mathcal{O}(\Delta t, h^2, k^2).
\end{aligned} \tag{28}$$

Proceeding similarly for the second equation of system (4) we obtain

$$\tilde{v}_0^{n+1} = \tilde{v}_0^n\Big[1 - \Delta t\,(1+m_{00})\Big] + \Delta t\cdot a\tilde{u}_0^n + \Delta t\sum_{i=1}^{s} m_{0i}\tilde{v}_i^n + \mathcal{O}(\Delta t, h^2, k^2), \tag{29}$$

and therefore, by definition of $\tilde{u}^n$ and $\tilde{v}^n$, taking maximums yields

$$\tilde{v}^{n+1} \le \Delta t\cdot\ a\tilde{u}^n + \Big[\Big|1 - \Delta t(1+m_{00})\Big| + \Delta t\sum_{i=1}^{s}|m_{0i}|\Big]\tilde{v}^n + \mathcal{O}(\Delta t, h^2, k^2). \tag{30}$$

Inequalities (28) and (30) can be rewritten as

$$\begin{pmatrix} \tilde{u}^{n+1} \\ \tilde{v}^{n+1} \end{pmatrix} \le \begin{pmatrix} M_{11} & M_{12} \\ M_{21} & M_{22} \end{pmatrix}\begin{pmatrix} \tilde{u}^n \\ \tilde{v}^n \end{pmatrix} + \mathcal{O}(\Delta t, h^2, k^2), \tag{31}$$

where M_{21} and M_{22} are the coefficients in (30) and M_{11}, M_{12} are given by

$$M_{11} = \Big|1 - \Delta t\cdot D\,m_{00}\Big| + \Delta t\cdot D\sum_{i=1}^{s}|m_{i0}| + A_1\cdot\Delta t, \quad M_{12} = \Delta t\cdot B_1, \tag{32}$$

for the values of A_1 and B_1 considered in (23) and (24). Thus, the square matrix in (31) is

$$M := \begin{pmatrix} \left|1 - \Delta t \cdot D\, m_{00}\right| + \Delta t \cdot D \sum_{i=1}^{s} |m_{i0}| + A_1 \cdot \Delta t & \Delta t \cdot B_1 \\ \Delta t \cdot a & \left|1 - \Delta t(1 + m_{00})\right| + \Delta t \sum_{i=1}^{s} |m_{i0}| \end{pmatrix}. \tag{33}$$

To complete the proof, having obtained expression (31), we impose a condition on the norm of the matrix M to prove that the errors converge to zero as $n \to \infty$. Specifically, we employ the $\|\cdot\|_1$ norm, defined as the maximum absolute row sum of M, and require that $\|M\|_1 < 1$.

If, on the one hand, we have

$$\|M\|_1 = \left|1 - \Delta t \cdot Dm_{00}\right| + \Delta t \cdot D \sum_{i=1}^{s} |m_{i0}| + A_1 \cdot \Delta t + \Delta t \cdot B_1,$$

then, $\|M\|_1 < 1$ is equivalent to

$$\left|1 - \Delta t \cdot Dm_{00}\right| < 1 - \Delta t \cdot D \sum_{i=1}^{s} |m_{i0}| - A_1 \cdot \Delta t - \Delta t \cdot B_1,$$

which holds since we imposed condition (25), which includes

$$\Delta t < \frac{2}{Dm_{00} + D\sum_{i=1}^{s} |m_{i0}| + A_1 + B_1}.$$

Otherwise, if the contrary is true, this is

$$\|M\|_1 = \Delta t \cdot a + \left|1 - \Delta t(1 + m_{00})\right| + \Delta t \sum_{i=1}^{s} |m_{i0}|,$$

then $\|M\|_1 < 1$ is equivalent to,

$$\left|1 - \Delta t(1 + m_{00})\right| < 1 - \Delta t \cdot a - \Delta t \sum_{i=1}^{s} |m_{i0}|,$$

which again holds under the assumption (25) in Theorem 1, as in particular

$$\Delta t < \frac{2}{1 + m_{00} + \sum_{i=1}^{s} |m_{i0}| + a}.$$

6. Numerical study

Making use of the GFD scheme (22) developed in Section 5, we next turn to compute numerical approximations of the solution of system (4). In order to assess the different cases studied throughout the article, we consider various choices of f. First a constant supply is considered, including both the case $r > f$ and $r < f$. Then, the asymptotic periodicity of solutions is studied for time-periodic supplies, including average values above and below r. In addition, we also include a section concerning pattern formation, as well as a final numerical estimate of the order of convergence of the method.

For clarity of presentation, although the GFD method has been formulated in two spatial dimensions, all numerical simulations are performed on a one-dimensional domain. This allows for simpler visualization of the results without loss of generality, since the method and its implementation can be easily extended to higher dimensions.

Throughout the simulations, we consider the following parameter set, unless otherwise stated

$$D = 0.5, \quad \chi = 2, \quad r = 1, \quad a = 1, \tag{34}$$

under different choices of the external supply $f(x,t)$.

We take the one-dimensional domain $\Omega := (0,1)$ and a set of 40 nodes unevenly distributed over the interval. The weights we considered as dist^{-4}, and the time step as $\Delta t = 2.5 \cdot 10^{-4}$, which is small enough to grant the convergence of the scheme for the chosen discretization of Ω.

6.1. Constant external supplies

We begin by investigating the dynamics of system (4) under constant supply rates, with $f(x,t) \equiv f$. As determined in Section 2, the balance between r and f determines the linearized dynamics of the system.

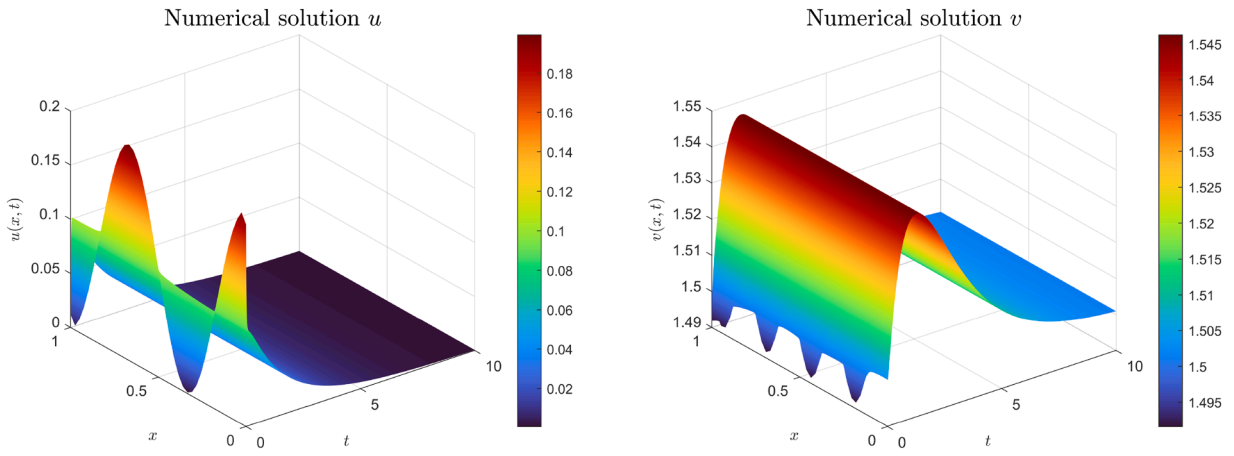

Fig. 1. Numerical solution to system (4) with parameters (34), $f = 1.5 > r$, and initial values (35).

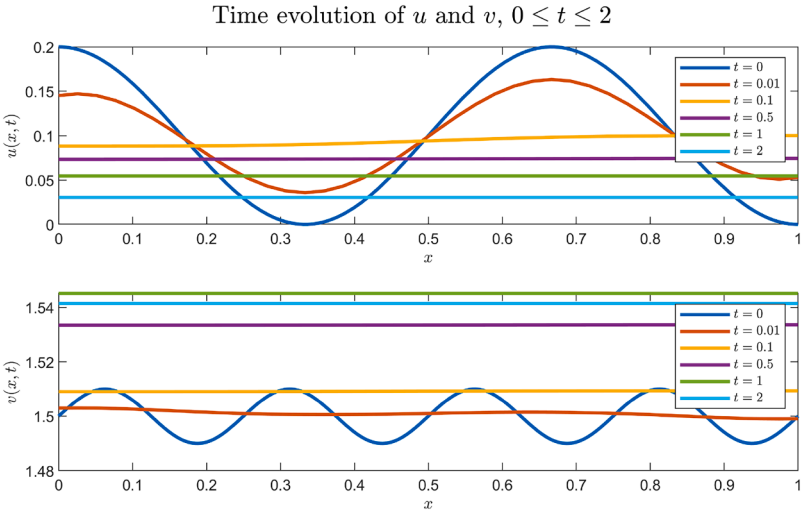

Fig. 2. Different time profiles of the solution represented in Fig. 1. The u component of the solution is represented in the top panel, with the v component in the bottom panel.

6.1.1. *The case $r < f$*

Our analysis starts by considering a sufficiently large external supply of the substance, satisfying $r < f$. In this case, the only biologically meaningful spatially homogeneous steady state is $(0, f)$, which is locally asymptotically stable. For this purpose, we choose for instance

$$f(x,t) \equiv 1.5 > 1 = r,$$

and initialize the system with $u(x,0)$ and $v(x,0)$ taken as small perturbations of $(0, f)$.

Since the selected supply rate f is greater than the logistic growth rate r, we expect the concentration of the substance to attain sufficiently high levels, so that the cell death term $-uv$ dominates bacterial proliferation, ultimately driving the solution back toward $(0, f)$.

We consider the following initial values

$$u(x,0) = 0.1 \cdot (1 + \cos(3\pi x)), \quad v(x,0) = 1.5 + 0.01 \cdot \sin(8\pi x), \tag{35}$$

close to $(0, f) = (0, 1.5)$. We solve the equations using the GFD scheme (22) until $t = 10$. Fig. 1 depicts the spatial and temporal evolution of the numerical solutions for this case. The one-dimensional spatial setting allows for a three-dimensional representation of the solution, with time advancing to the right. For a better representation of the initial dynamics of the system, different time profiles for $0 \le t \le 2$ are also represented in Fig. 2.

As can be seen in both images, the oscillatory shape of the initial values $u(x,0)$ and $v(x,0)$ is rapidly lost due to diffusion, with both u and v rapidly flattening before $t = 0.5$. In the case of the bacterial population u, as expected, the overall high concentrations of the substance effectively prevent its growth, and the solution converges uniformly to zero. With respect to v, the large supply induces a

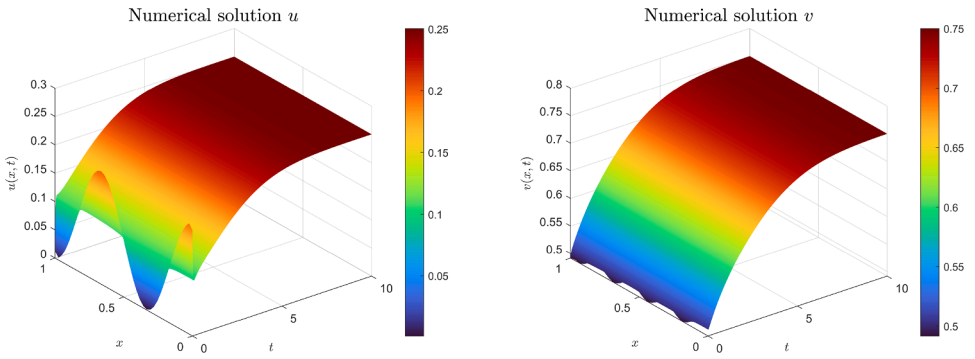

Fig. 3. Numerical solution to system (4) with parameters (34), $f = 0.5 < r$, and initial values (35).

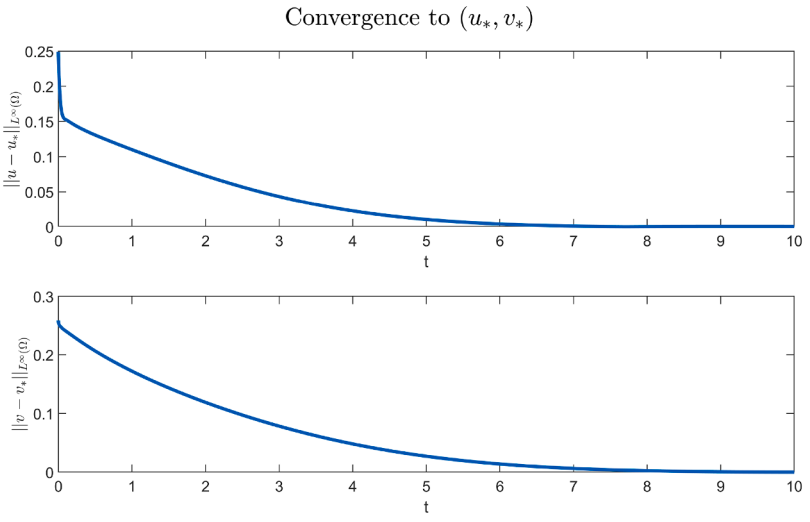

Fig. 4. Convergence of the solution represented in Fig. 3 to the steady state $(u_*, v_*) = (0.25, 0.75)$ in $L^\infty(\Omega)$ norm.

steep initial increase —visible in the bottom panel of Fig. 2— which is soon compensated as the degradation term $-v$ becomes larger, decaying uniformly in time to the steady state, $v = f = 1.5$.

6.1.2. *The case $r > f$*

Next, we explore the case $r > f$, which admits two different nonnegative spatially homogeneous steady states, the previous one $(0, f)$, as well as the coexistence state (u_*, v_*) given in (7). To illustrate this case, we consider the same parameter set (34), this time taking

$$f(x,t) \equiv 0.5 < 1 = r.$$

In this regime, the logistic growth rate dominates the supply of the substance, which makes $(0, f)$ unstable, and (u_*, v_*) locally asymptotically stable. To study both equilibria, we compute two numerical solutions of the system, using initial values close to these steady states.

First, for studying the dynamics close to $(0, f)$, we consider the same initial values from the previous case, given by (35), and analyze the differences that arise. As in this case the equilibrium $(0, f)$ becomes unstable, we expect that the change in the supply rate f results in a solution that moves away from $(0, f)$ and possibly converges to (u_*, v_*), which is in turn locally asymptotically stable.

Computing again the solution using the GFD scheme (22) and the same node distribution yields the outcome depicted in Fig. 3.

The results in Fig. 3 agree with the expected behavior. Since the logistic growth rate r is significantly larger than the external supply f, the bacterial population rapidly proliferates, approaching the coexistence level $u_* = 0.25$. For the substance concentration v, the combined effect of the constant external supply and bacterial self-production overcome the degradation term, leading to an increase toward the equilibrium value $v_* = 0.75$. As in the previous case, the spatial oscillations from the initial values are quickly suppressed by diffusion for both components. This initial smoothing is followed by a growth phase, during which the solution approaches (u_*, v_*) until approximately $t = 5$, after which the solution keeps gradually converging to the equilibrium.

To analyze this convergence to (u_*, v_*), the time evolution of $||u(.,t) - u_*||_{L^\infty(\Omega)}$ and $||v(.,t) - v_*||_{L^\infty(\Omega)}$ is represented in Fig. 4.

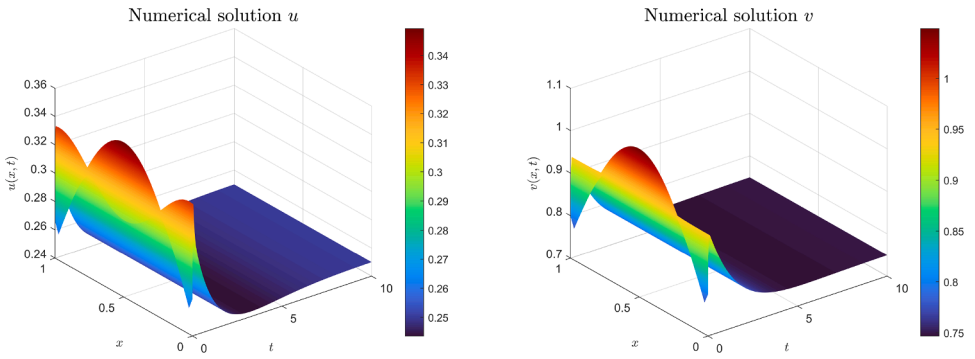

Fig. 5. Numerical solution to system (4) with parameters (34), $f = 0.5 < r$, and initial values (36).

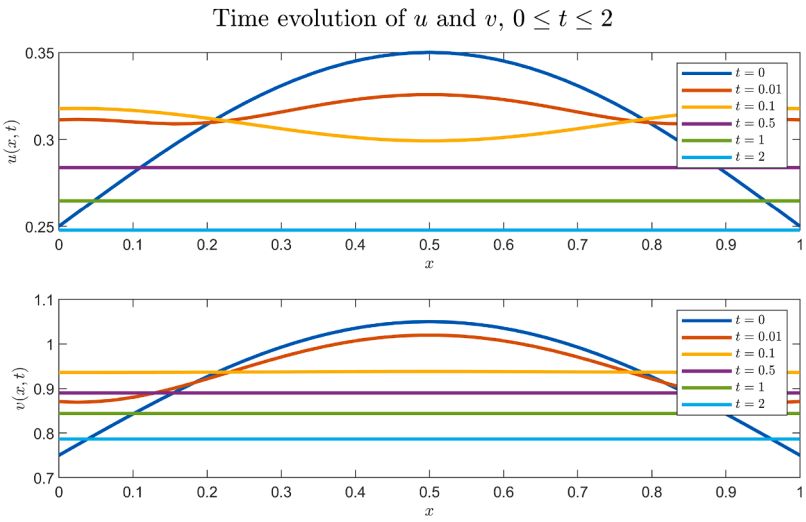

Fig. 6. Different time profiles of the solution represented in Fig. 5. The u component of the solution is represented in the top panel, with the v component in the bottom panel.

As can be seen on both panels, the previously described growth phase occurs during the first 5 time instants, as reflected by the decrease in the norms. From then on, both $||u(.,t) - u_*||_{L^\infty(\Omega)}$ and $||v(.,t) - v_*||_{L^\infty(\Omega)}$ remain close to 0, indicating the convergence to the steady state.

Next, we consider two initial values close to the coexistence equilibrium (u_*, v_*) in order to assess its local asymptotic stability. To explore the resulting dynamics, we take for instance

$$u(x,0) = u_* + 0.1 \cdot \sin(\pi x), \quad v(x,0) = v_* + 0.3 \cdot \sin(\pi x), \tag{36}$$

again with parameters (34) and $f(x,t) \equiv 0.5 < 1 = r$. Since both initial data attain their maximum at the center of the domain, at $x = 1/2$, negative chemotaxis will drive bacteria away from this region, leading them toward the sides. From then on, we again expect diffusion to flatten the shape of the solutions, while returning asymptotically to (u_*, v_*).

The results for this scenario are shown in Fig. 5. As in the first case, to better illustrate these dynamics at short time scales, several time profiles of the solution are represented in Fig. 6.

As shown in Fig. 5, since both initial values lie above u_* and v_*, the corresponding solutions experience a time decay toward the coexistence equilibrium (u_*, v_*), to which they uniformly converge.

On short time scales, the dynamics are strongly influenced by chemotaxis. At $t = 0.01$, represented in red in Fig. 6, the initial shape of u has already been significantly altered, with an increase of the bacterial density near the boundaries and a considerable reduction at $x = 1/2$, which, however, still hosts the maximum bacterial density. By $t = 0.1$, depicted in yellow, this chemotaxis-driven migration is completed, with the center of the domain having the lowest bacterial concentration. From then on, the density is homogenized throughout the domain due to diffusion, being progressively reduced while converging to $u_* = 0.25$.

Regarding the substance concentration v, by $t = 0.1$, diffusion has already flattened the shape of the solution, which similarly approaches $v_* = 0.75$ as time passes.

For the study of the convergence, the time evolution of $||u(.,t) - u_*||_{L^\infty(\Omega)}$ and $||v(.,t) - v_*||_{L^\infty(\Omega)}$ are represented in Fig. 7.

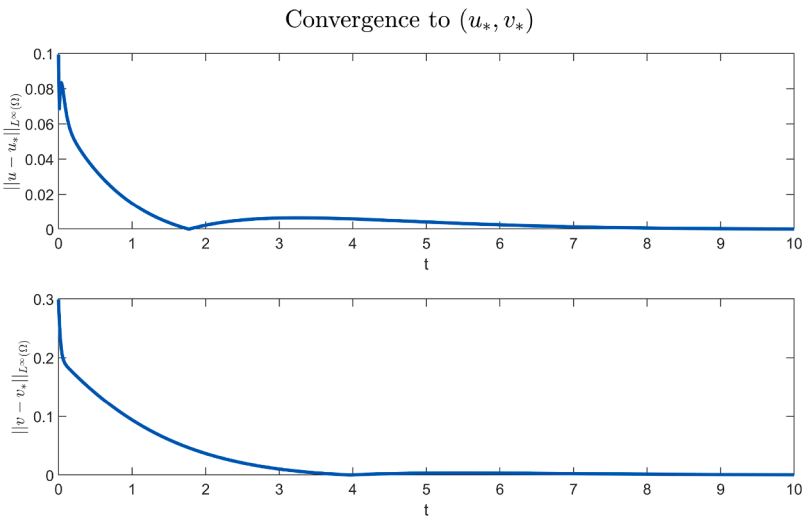

Fig. 7. Convergence of the solution represented in Fig. 5 to the steady state $(u_*, v_*) = (0.25, 0.75)$ in $L^\infty(\Omega)$ norm.

It is worth noting that both solutions actually achieve their corresponding steady state value, u_* and v_*, independently at a finite time. For u, this occurs shortly before $t = 2$, while for v it is close to $t = 4$. However, as the equilibrium values are not reached simultaneously, the solution keeps evolving, until for larger values of t, both u and v asymptotically converge to u_* and v_*

6.2. Periodicity

Having studied the dynamics of system (4) for constant values of f, we now turn to time-periodic supplies, with the aim of describing the resulting asymptotically periodic regime.

6.2.1. The case $a = 0$

We first consider the case $a = 0$, for which the threshold $r_{\min}$ was characterized in (17). We recall that for a given $T-$periodic function $\hat{f}(t)$ —to which f converges in time— if its average value over one period exceeds the logistic growth rate r, then the solution $(\tilde{u}, \tilde{v})$ of system (5) satisfies $\tilde{u} \to 0$ as $t \to \infty$. If, on the other hand the average of $\hat{f}$ is less than r, there exists a unique positive $T-$periodic solution to system (5) characterized by the initial values (13) and (15), to which any other solution with positive initial values converges.

Since for any pair of initial values $u(x, 0)$ and $v(x, 0)$, the solution (u, v) to the original PDE system (4) is known to converge in time to the solution of the associated ODE system (5) with initial values (6), the asymptotic periodic behavior of solutions to system (4) in the case $a = 0$ is fully characterized by the threshold $r_{\min}$.

To begin the numerical study, we first consider the time-periodic supply

$$f(x, t) = 0.5 \cdot \left[1 + \cos(\pi t)\right], \tag{37}$$

of period $T = 2$, and the parameter set (34), except for a, which we keep fixed at $a = 0$.

To determine wether f induces a periodic response in the system or not, we compute the threshold $r_{\min}$ from (17). For this choice of f, as it is directly spatially homogeneous, we have $\hat{f} = f$, and thus

$$r_{\min} = \frac{1}{T}\int_0^T \hat{f}(s)\, ds = \frac{1}{2}\int_0^2 0.5 \cdot \left[1 + \cos(\pi s)\right] ds = 0.5.$$

As the logistic growth rate of the species satisfies $r = 1 > 0.5 = r_{\min}$, the solution to system (4) will asymptotically reach a periodic regime for any positive pair of initial values $u(x, 0)$ and $v(x, 0)$. To characterize this periodic regime, we determine the initial values $(\tilde{u}_0, \tilde{v}_0)$ for the ODE system, as given in (13) and (15). First

$$\tilde{v}_0 = \frac{1}{e^T - 1}\int_0^T \hat{f}(s) e^s\, ds = \frac{1}{2}\left(1 + \frac{1}{\pi^2 + 1}\right), \tag{38}$$

and with it

$$\tilde{v}(t) = \frac{1}{2}\left(1 + \frac{1}{\pi^2 + 1}\left(\pi \sin(\pi t) + \cos(\pi t)\right)\right). \tag{39}$$

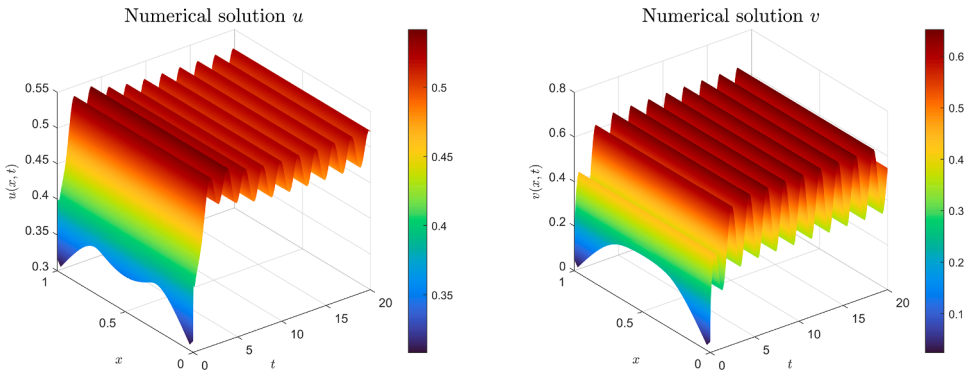

Fig. 8. Numerical solution to system (4) with parameters (34) except for $a = 0$, $f(x,t)$ in (37) (satisfying $r > r_{\min}$) and initial values (41).

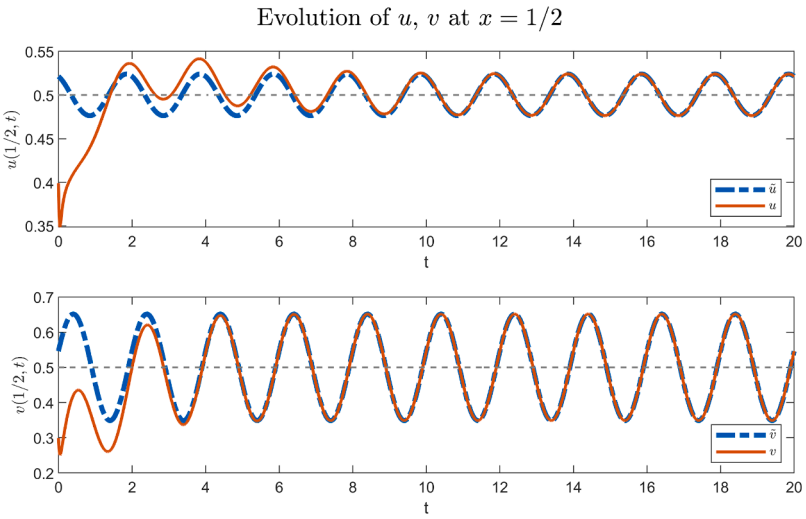

Fig. 9. Convergence of the solution (u, v) from Fig. 8 to $(\tilde{u}, \tilde{v})$ at $x = 1/2$.

This allows us to compute $\tilde{u}_0$ as

$$\tilde{u}_0 = \frac{e^{\int_0^T (r - \tilde{v}(s))\, ds} - 1}{\int_0^T \left(r\, e^{\int_0^s (r - \tilde{v}(\tau))\, d\tau} \right) ds} \approx 0.5214 \tag{40}$$

To study how the numerical solution to the PDE system converges to the unique positive periodic solution $(\tilde{u}, \tilde{v})$ of the ODE system (5) generated by (38) and (40), we select a pair of initial values. For instance, similar to those of the previous example, we consider

$$u(x,0) = 0.3 + 0.1 \cdot \sin(\pi x), \quad v(x,0) = 0.3 \cdot \sin(\pi x). \tag{41}$$

The evolution of u and v is depicted in Fig. 8, where the asymptotic periodicity can already be observed.

To better analyze the transition toward the periodic regime and the convergence of (u, v) to $(\tilde{u}, \tilde{v})$, we fix $x = 1/2$ and plot in Fig. 9 the time evolution of u and v at said coordinate.

Given the shape of the initial bacterial and substance distributions —with both having a maximum precisely at $x = 1/2$— as in previous case, the bacterial population migrate away from the center of the domain, as reflected by the sudden decrease of $u(1/2,t)$ in the first instants. Diffusion causes $v(1/2,t)$ to also decrease initially, albeit less intensely. From there on, the logistic dynamics of the bacteria and the external supply of the substance boost the growth of both u and v. With r being sufficiently large, the bacteria soon grow until reaching a first maximum near $t = 2$. The death term $-uv$ prevents a greater increase of the population, which begins to oscillate, indicating the periodic response to the source. This translates into an eventual convergence to $\tilde{u}$, with both curves being nearly identical soon after $t = 8$. The convergence of v to $\tilde{v}$ is faster, having very similar values already at $t = 4$.

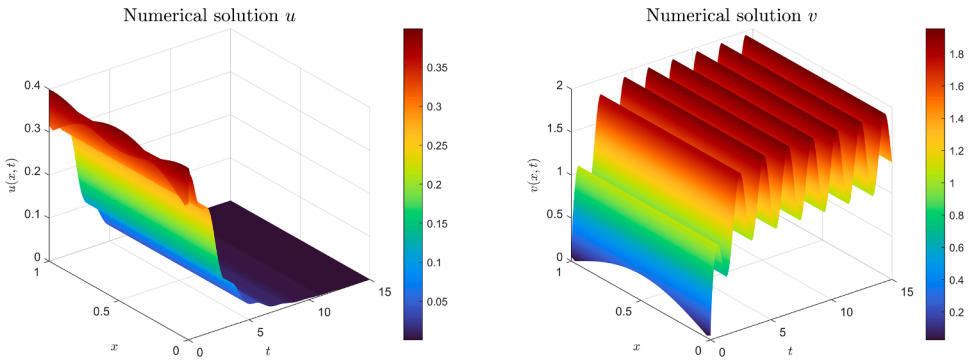

Fig. 10. Numerical solution to system (4) with parameters (34) except for $a = 0$, $f(x,t)$ in (42) (satisfying $r < r_{\min}$) and initial values (41).

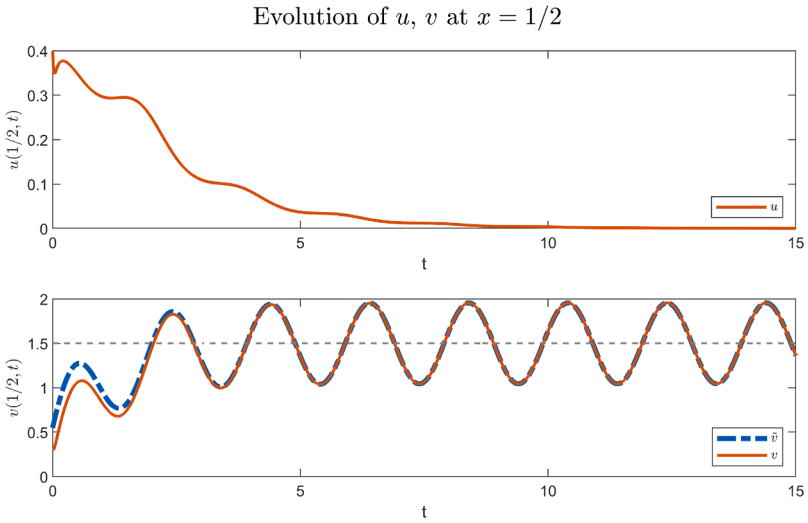

Fig. 11. Convergence of the solution (u, v) from Fig. 10 to $(\tilde{u}, \tilde{v})$ at $x = 1/2$.

In addition to the solution trajectories, the figure includes gray dashed horizontal lines corresponding to (u_*, v_*), the steady state (7), computed by taking the average of $\hat{f}$ as the constant supply rate. This shows that, in this periodic regime, the dynamics of the system are governed by oscillations around the equilibrium associated to a constant supply of the average value of $\hat{f}$.

Secondly, we consider the same biological setting, in terms of the parameter set (34) with $a = 0$ and the initial values (41), but with a new supply term, given by

$$f(x,t) = 1.5 \cdot \big[1 + \cos(\pi t)\big]. \tag{42}$$

This choice of f entails the same periodic structure as the previous one considered in (37), but with a larger amplitude factor. Again, since f contains no spatial heterogeneities, we have $\hat{f} = f$, with a corresponding threshold value of

$$r_{\min} = \frac{1}{2}\int_0^2 1.5 \cdot \big[1 + \cos(\pi s)\big]\, ds = 1.5.$$

Hence, only a species with a logistic growth rate above $r_{\min} = 1.5$ can sustain a periodic regime of the type described above. For this case, however, as $r = 1 < r_{\min}$, the largeness of f is expected to drive the population to zero due to the high concentration of the substance.

The corresponding numerical solution is shown in Fig. 10. As expected, instead of converging to a time-periodic solution, the bacterial density u suffers an oscillating decay. In this regime, the logistic growth of the species is insufficient to compensate for the high concentrations that the substance reaches, which induce a strong death term $-uv$.

In contrast, the periodicity of f is inherited only by the substance concentration v, which asymptotically reaches a periodic regime, as can be deduced from the explicit expression for $\tilde{v}$ given in (12), which is independent of r. This can be further visualized in Fig. 11, where the time evolution of u and v is depicted at the fixed coordinate $x = 1/2$, showing on the one hand the decay for u and on the other hand the asymptotic periodicity for v.

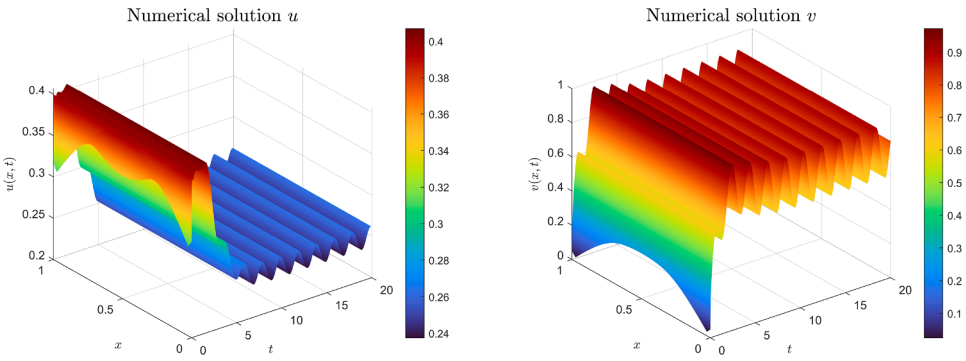

Fig. 12. Numerical solution to system (4) with parameters (34), $f(x,t)$ in (37) and initial values (41).

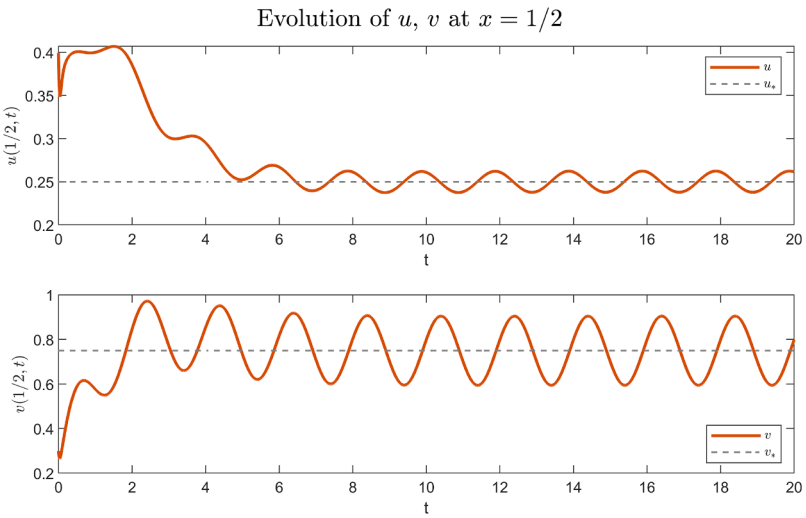

Fig. 13. Convergence to periodic solutions at $x = 1/2$.

6.2.2. The case $a > 0$

To complete the study of the periodic dynamics, we consider one example with $a > 0$, where the substance is self-produced by the bacteria. While time convergence of (u, v) to $(\tilde{u}, \tilde{v})$ still holds uniformly in Ω, explicit threshold conditions characterizing the periodicity of $(\tilde{u}, \tilde{v})$ are still lacking.

We take the full parameter set (34) (again with $a = 1$), the initial values (41) and the supply f considered in (37), which resulted in asymptotically periodic behavior for the case $a = 0$.

The numerical solutions are represented in Fig. 12, again with the time evolution at $x = 1/2$ in Fig. 13, including the reference values (u_*, v_*) computed again by taking again the average of $\hat{f}$ over one period as a constant supply.

As can be seen in both figures, both u and v again appear to converge toward an asymptotically periodic regime, although with stark contrast to the results obtained for this same scenario with $a = 0$, depicted in Fig. 8. In the present case, the positive value of a results in a decrease of the associated value of u_*, from the previous 0.5 for $a = 0$ to the current 0.25. Consequently, since the initial value $u(x, 0)$ now lies significantly above u_*, after a short time span in which chemotaxis governs the dynamics of the system, u experiences a decrease until approaching u_*, around which the periodic oscillations are centered.

For the substance concentration v, the self-production term leads to overall higher results, nearly reaching 1 at $x = 1/2$, shortly after $t = 2$, at the time when the bacterial density is also at its maximum. The associated value of v_* is now higher as well, from 0.5 for $a = 0$ to 0.75 in this case.

Thus, the periodicity induced by the supply f is preserved for this case with $a > 0$. However, the self-production of the substance alters the periodic regime by increasing the average substance concentration, which in turn results in a decrease in the level around which the bacterial density oscillates.

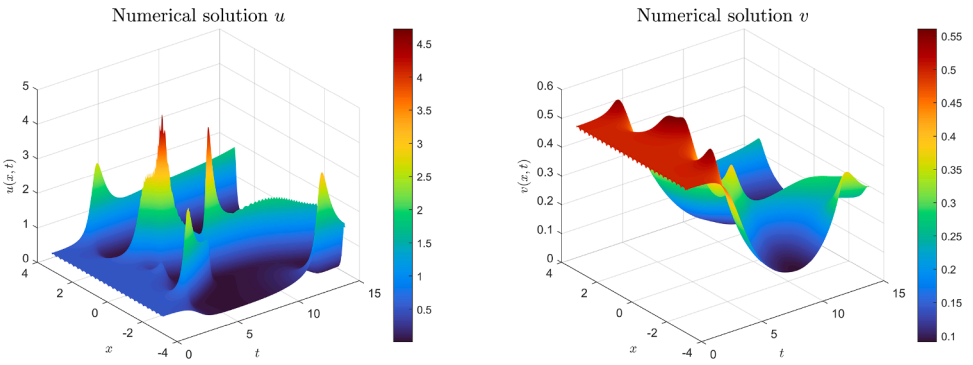

Fig. 14. Numerical solution to system (4) with parameter values (43) and initial values (44).

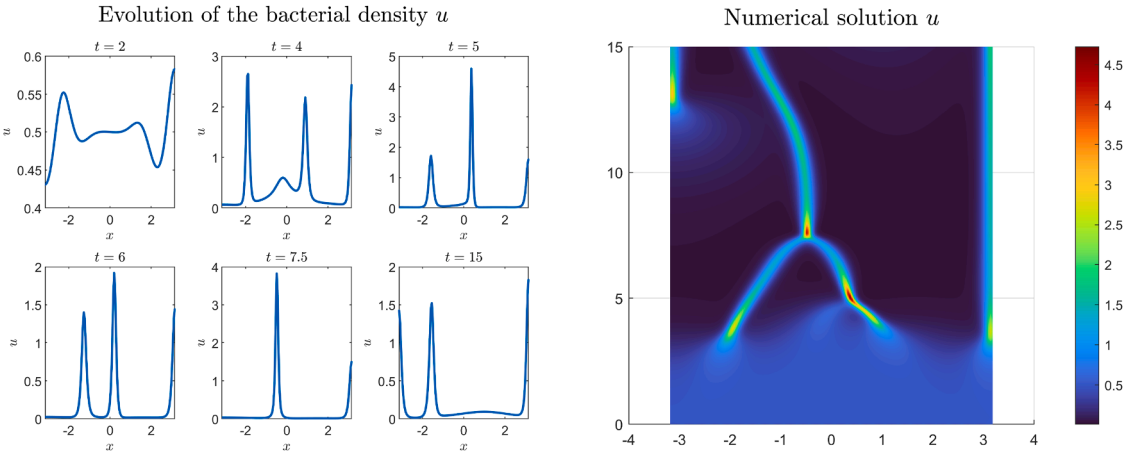

Fig. 15. Evolution of the u component of the solution from Fig. 14.

6.3. Arising patterns

Lastly, we devote this section to show some spatial patterns that can be generated by system (4) under certain parameter configurations, when local stability is not preserved. The topic of pattern formation in chemotaxis systems has been widely studied, for instance in [30], where a large range of one-dimensional patterns are described.

To obtain meaningful results, we consider a longer domain, in this case $\Omega = (-\pi, \pi)$ and first take the following parameters

$$D = 0.1, \quad \chi = 9, \quad r = 1, \quad a = 1, \quad f(x,t) \equiv 0. \tag{43}$$

Notice that in this case the process in mainly chemotaxis-driven, due to the largeness of χ. As initial values, we consider a small perturbation around $(u^*, v^*) = (0.5, 0.5)$, given by

$$u(x,0) = u^* = 0.5, \quad v(x,0) = v^* + 0.01 \cdot \sin(8x) = 0.5 + 0.01 \cdot \sin(8x). \tag{44}$$

The numerical solution up to $t = 15$ is represented in Fig. 14. Focusing on the bacterial density u, we observe the formation of localized clusters of bacteria with high population densities, while other regions of the domain remain nearly empty.

To better illustrate the emergence, interaction, and merging of these clusters, Fig. 15 represents several time profiles of the solution u, together with a vertical view of the left panel in Fig. 14.

We observe that until $t = 2$, the solution remains close to the homogeneous equilibrium u^*, with different small aggregations whose amplitudes are bounded between 0.4 and 0.6. From this time onward, certain peaks start to emerge, as can be seen at the left panel at $t = 4$. The highest bacterial concentrations are located near $x = -2$, $x = -0.5$, $x = 1$ and the boundary $x = \pi$.

The two central peaks eventually merge into a single aggregate, shortly before $t = 5$, which can be better visualized in the right diagram. The remaining two interior clusters merge again before $t = 7.5$. At this stage, the bacterial density at the center of the resulting cluster is nearly 4, significantly exceeding the carrying capacity of the logistic model, which is normalized to 1. As a result, the population density subsequently decreases.

Finally, a third peak emerges near the left boundary $x = -\pi$ after $t = 12$, as shown in the right panel, which can also be seen in the final profile at $t = 15$, where all population densities have already fallen below 2.

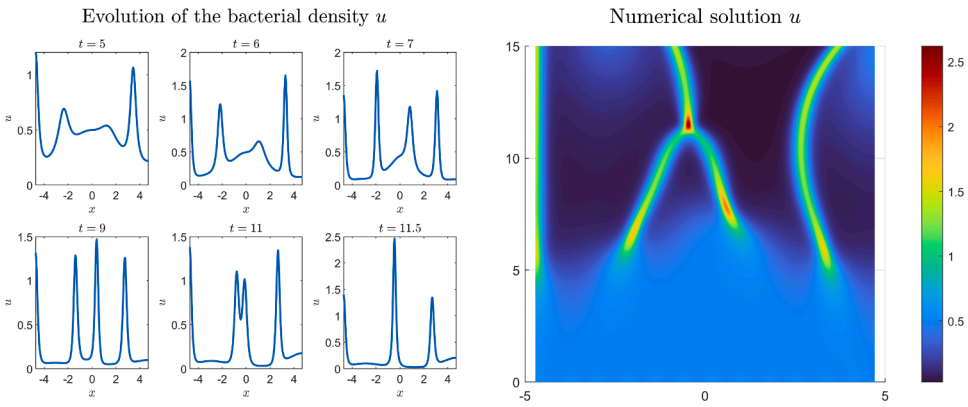

Fig. 16. Numerical solution to system (4) with parameter values (43) and initial values (44).

Table 1
Maximum error in l^∞ for three different meshes and numerical order of convergence.

Number of nodes	l^∞ norm of the error	O.C.
10	0.00114	-
19	$5.4183 \cdot 10^{-4}$	2.103
37	$2.0811 \cdot 10^{-4}$	2.603

Similar patters also arise when considering a larger domain, for instance by considering $\Omega = (-\frac{3\pi}{2}, \frac{3\pi}{2})$, with the same parameters as in (43), except for $\chi = 6$. The results are represented once again in Fig. 16, only for the u component of the solution, with different time profiles on the left panel and a vertical view on the right one.

Though at the initial stages, up to approximately $t = 5$, the solution does not present great spatial heterogeneity, four distinct bacterial clusters eventually emerge, shortly before $t = 7$. First, one near the left boundary; two at the center of the domain, which subsequently merge into a single aggregate at around $t = 11.5$, and a fourth one on the right half of the domain. Due to the lower value of χ compared to the previous case, these aggregations do not attain the same high population densities. In particular, the bacterial density remains below 2.5 throughout the simulation –reached when both central clusters merge– whereas previously the maximum value was slightly below 5.

6.4. Numerical order of convergence

As a final remark, in this last subsection we numerically estimate the order of convergence (O.C.) of the proposed scheme. We compare an artificial solution over three different meshes with 10, 19 and 37 nodes, yielding the results in Table 1, where we see that the estimated order of convergence is close to its actual value, 2.

7. Conclusions

Throughout this paper, a mathematical model describing the interaction between a biological species and a chemical substance, was presented and analyzed. The model, governed by system (4), incorporates cell motility, negative chemotaxis, and logistic growth for the bacterial population, together with lethality induced by the substance and an external supply term.

The local stability of the spatially homogeneous steady states was studied in Section 2 for constant supply rates f. Two different equilibria, $(0, f)$ and (u_*, v_*), given in (7), were obtained. The coexistence equilibrium (u_*, v_*) is biologically meaningful only when the logistic growth rate r satisfies $r > f$. In this regime, as the growth rate of the species exceeds the external supply, the state $(0, f)$ is unstable, whereas (u_*, v_*) is locally asymptotically stable. Conversely, if $r < f$, the external supply dominates the bacterial growth, and $(0, f)$ becomes locally asymptotically stable, with any bacterial proliferation being suppressed by the high concentration of the chemical substance.

In Section 3, the case of an asymptotically time-periodic source function f was studied, through a reduction to the associated ODE system (5). In the absence of self-production of the substance by the bacteria (that it, the case $a = 0$), an explicit expression for the second component $\tilde{v}$ could be obtained, which allowed us to characterize the initial conditions leading to periodic solutions. Moreover, a threshold value $r_{\min}$, defined in (17), was obtained, in terms of the average of the periodic supply over one period. This threshold guarantees the existence of a unique positive T-periodic solution to the ODE system whenever $r > r_{\min}$, constructed by means of the initial data (13) and (15). Under these conditions, solutions of the full PDE system converge asymptotically in time to this periodic regime. If, on the contrary, $r \leq r_{\min}$ no such solution exists, leading the bacterial density u to a time decay toward extinction.

The remainder of the paper was devoted to numerical investigations. In Section 4, a brief introduction to the Generalized Finite Difference (GFD) method is provided, which we employ to approximate the solution of the model. The explicit numerical scheme (22) was presented in Section 5, together with a stability condition on the time step ensuring convergence, established in Theorem 1.

Numerical simulations presented in Section 6 confirm the analytical results on linear stability and periodic behavior obtained in the previous section. In particular, the stability properties of the equilibria for the cases $r < f$ and $r > f$ were illustrated in Figs. 1–2, and Figs. 3–7, respectively. The convergence toward time-periodic solutions was also demonstrated numerically, first for $a = 0$ both in the regime $r > r_{\min}$, where solutions converge to a positive periodic orbit (Fig. 9), and in the case $r < r_{\min}$, where the bacterial population exhibits an oscillatory decay (Fig. 11), as well as for $a > 0$, where asymptotic periodicity was also obtained (Fig. 13). Finally, qualitative observations on pattern formation in the full PDE system and numerical convergence properties of the scheme were reported in Figs. 14–16 and Table 1, respectively.

CRediT authorship contribution statement

Federico Herrero-Hervás: Writing – review & editing, Software, Investigation, Formal analysis; **Mihaela Negreanu:** Writing – review & editing, Supervision, Investigation, Funding acquisition, Formal analysis, Conceptualization.

Data availability

No data was used for the research described in the article.

Declaration of competing interest

The authors declare that they have no known competing financial interests or personal relationships that could have appeared to influence the work reported in this paper.

Acknowledgement

This work was supported by Project PID2022-141114NB-I00 by Ministerio de Ciencia e Innovación (Spain) and by Grant FPU23/03170 (F.H-H.) from the Spanish Ministry of Science, Innovation and Universities.

References

[1] Kumar R, Imlay S, J A. How escherichia coli tolerates profuse hydrogen peroxide formation by a catabolic pathway. J Bacteriol 2013;195(20):4569–79.
[2] Seaver LC, Imlay JA. Hydrogen peroxide fluxes and compartmentalization inside growing escherichia coli. J Bacteriol 2001;183.
[3] Benov L, Fridovich I. Escherichia coli exhibits negative chemotaxis in gradients of hydrogen peroxide, hypochlorite, and n-chlorotaurine: products of the respiratory burst of phagocytic cells. Proc Natl Acad Sci USA 1996;93(10):4999–5002.
[4] Uhl L, Gerstel A, Chabalier M, Dukan S. Hydrogen peroxide induced cell death: one or two modes of action? Heliyon 2015;1(4).
[5] Imlay JA, Linn S. Bimodal pattern of killing of dna-repair-defective or anoxically grown escherichia coli by hydrogen peroxide. J Bacteriol 1986;166(2).
[6] Cundliffe E, Demain AL. Avoidance of suicide in antibiotic-producing microbes. J Ind Microbiol Biotechnol 2010;37(7):643–72.
[7] Keller EF, Segel LA. Initiation of slime mold aggregation viewed as an instability. J Theoret Biol 1970;26:399–415.
[8] Keller EF, Segel LA. A model for chemotaxis. J Theoret Biol 1971;30:225–34.
[9] Bellomo N, Bellouquid A, Tao Y, Winkler M. Toward a mathematical theory of keller-segel models of pattern formation in biological tissues. Math Model Methods Appl Sci 2015;25:1663–763.
[10] Hillen T, Painter KJ. A users guide to pde models for chemotaxis. J Math Biol 2009;58:183–217.
[11] Horstmann D. From 1970 until present: the keller-segel model in chemotaxis and its consequences. Jahresbericht der Deutschen Mathematiker-Vereinigung 2003;105(3):103–65.
[12] Bai X, Winkler M. Equilibration in a fully parabolic two-species chemotaxis system with competitive kinetics. Indiana Univ Math J 2016;65(2):553–83.
[13] Mizukami M. Boundedness and asymptotic stability in a two-species chemotaxis-competition model with signal-dependent sensitivity. Discrete and Continuous Dynamical Systems - B; vol. 22. 2017.
[14] Zhang Q, Li Y. Global solutions in a high-dimensional two-species chemotaxis model with lotka-volterra competitive kinetics. J Math Anal Appl 2018;467(1):751–67.
[15] Tello JI, Winkler M. Stabilization in a two-species chemotaxis system with logisitc source. Nonlinearity 2012;25:1413–25.
[16] Stinner C, Tello JI, Winkler M. Competitive exclusion in a two-species chemotaxis model. J Math Biol 2014;68(7):1607–26.
[17] Herrero-Hervás F, Negreanu M. Asymptotics and periodic dynamics in a negative chemotaxis system with cell lethality. 2025. Preprint.
[18] Benito JJ, García A, Gavete L, Negreanu M, na FU, Vargas AM. Solving a fully parabolic chemotaxis system with periodic asymptotic behavior using generalized finite difference method. Appl Numer Math 2020;157:356–71.
[19] Benito JJ, García A, Gavete L, Negreanu M, na FU, Vargas AM. Solving a chemotaxis-haptotaxis system in 2d using generalized finite difference method. Comput Math Appl 2020;80(5):762–77.
[20] Benito JJ, García A, Gavete L, Negreanu M, na FU, Vargas AM. On the convergence of the generalized finite difference method for solving a chemotaxis system with no chemical diffusion. 2020, https://doi.org/10.1007/s40571-020-00359-w
[21] Herrero-Hervás F, Negreanu M, Vargas AM. Convergence of a meshless numerical method for a chemotaxis system with density-suppressed motility. Comput Mathe Appl 2023;148:293–301.
[22] Herrero-Hervás F. An explicit-implicit generalized finite difference scheme for a parabolic-elliptic density-suppressed motility system. J Comput Appl Math 2024;446.
[23] Drangeid AK. The principle of linearized stability for quasilinear parabolic evolution equations. Nonlinear Anal; vol. 13. 1989.
[24] Dáger R, Navarro V, Negreanu M, Vargas AM. Uniform asymptotic behavior of numerical solutions for a predator-prey system with diffusion and chemotaxis. Eng Anal Bound Elem 2020;120:82–94.
[25] Negreanu M, Vargas AM. On a fully parabolic chemotaxis system with source term and periodic asymptotic behavior. Zeitschrift für angewandte Mathematik und Physik 2020;71.

[26] Negreanu M, Tello JI, Vargas AM. Continuous and discrete periodic asymptotic behavior of solutions to a competitive chemotaxis pdes system. Commun Nonlinear Sci Numer Simul 2021;95.
[27] Perrone N, Kao R. A general finite difference method for arbitrary meshes. Comput Struct 1975;5:45–58.
[28] Lancaster P, Salkauskas K. Curve and surface fitting. Ed Academic Press; 1986.
[29] Vargas AM. Finite difference method for solving fractional differential equations at irregular meshes. Math Comput Simul 2022;193:204–16.
[30] Painter KJ, Hillen T. Spatio-temporal chaos in a chemotaxis model. Physica D 2011;240:363–75.